Strong localization of Majorana end states in chains of magnetic adatoms

Yang Peng,[1] Falko Pientka,[1] Leonid I. Glazman,[2] and Felix von Oppen[1]

[1] *Dahlem Center for Complex Quantum Systems and Fachbereich Physik, Freie Universität Berlin, 14195 Berlin, Germany*
[2] *Department of Physics, Yale University, New Haven, CT 06520, USA*

A recent experiment [Nadj-Perge *et al.*, Science **346**, 602 (2014)] gives possible evidence for Majorana bound states in chains of magnetic adatoms placed on a superconductor. While many features of the observed end states are naturally interpreted in terms of Majoranas, their strong localization remained puzzling. We consider a linear chain of Anderson impurities on a superconductor as a minimal model and treat it largely analytically within mean-field theory. We explore the phase diagram, the subgap excitation spectrum, and the Majorana wavefunctions. Owing to a strong velocity renormalization, the latter are localized on a scale which is parametrically small compared to the coherence length of the host superconductor.

Introduction.—There is currently great interest in Majorana bound states in condensed-matter systems which realize nonabelian quantum statistics [1, 2] and may have applications in topological quantum information processing [3]. Several platforms allow one to engineer topological superconducting phases supporting Majorana bound states, based on proximity coupling to s-wave superconductors. These include topological insulators [4, 5], semiconductor quantum wires [6–8], and chains of magnetic adatoms [9–14] (see also [15–17]). All these proposals are being actively pursued in the laboratory [18–26].

A recent experiment [26] exhibits signatures of Majorana bound states in chains of Fe atoms placed on a Pb surface. Experiment suggests that the Fe chain orders ferromagnetically. The subgap spectrum is probed by scanning tunneling spectroscopy with both spatial and spectral resolution which shows zero-energy states near the ends of the chains. It is tempting to interpret these as Majorana bound states [26, 27] as the system combines the three essential ingredients: (i) Proximity-induced superconductivity; (ii) a finite Zeeman splitting due to the exchange field of the ferromagnetic Fe chains; and (iii) Rashba spin-orbit coupling (presumably from the surface of the Pb substrate).

However, the observed localization of the end states on the scale of a few adatom sites is puzzling [28, 29]. It is typically assumed that the localization length of Majorana states is larger than the coherence length ξ_0 of the proximity-providing superconductor since the induced topological gap is smaller than the gap of the host superconductor. In contrast, the observed localization length of the end states is orders of magnitude smaller than the superconducting coherence length of Pb. Here we address this puzzle by modeling the adatoms as a chain of Anderson impurities hybridized with a superconductor. We show that this model is amenable to a largely analytical solution within a standard mean-field approximation and gives rise to Majorana localization lengths which are parametrically smaller than ξ_0 over wide regions of parameter space.

The physics underlying the topological phase in chains of magnetic adatoms has been discussed in two approaches. One approach [9, 10, 30–32] starts with the subgap Shiba states [33–36] induced by the individual magnetic adatoms. The adatom is described as a classical magnetic moment which is exchange coupled to the electrons in the substrate, but otherwise electronically inert. Such Shiba chains exhibit topological superconducting phases and hence Majorana end states. An alternative approach [26, 27] starts with exchange-split adatom states. While they are far from the Fermi energy for individual adatoms, hopping between the adatoms of the chain broadens these states into bands. For sufficiently strong hopping, these bands cross the Fermi energy and effectively realize a one-dimensional spin-polarized electron system. In this band limit, topological superconductivity is induced by proximity, in combination with spin-orbit coupling for ferromagnetic chains or helical magnetic order along the chain.

In the Shiba limit, the spectral weight of the subgap excitations is entirely in the host superconductor. In the band limit, the spectral weight is divided between the adatom d levels and the superconductor, with the ratio depending on the hybridization strength. We show below that the transfer of spectral weight to the superconductor results in a stronger localization of the Majorana end states.

Model.—We model the system as a linear chain of Anderson impurities placed in an s-wave superconductor. Each adatom hosts a spin-degenerate level of energy ϵ_d with on-site Hubbard repulsion U, representing the Fe d-levels. We include nearest-neighbor hopping of strength w between these d-levels as well as hybridization of strength t between the d-levels and the superconductor. The model is described by the Hamiltonian

$$\mathcal{H} = \mathcal{H}_d + \mathcal{H}_s + \mathcal{H}_T, \tag{1}$$

where $\mathcal{H}_s$ is a BCS Hamiltonian of the superconductor, and the chain of d-levels is described by

$$\mathcal{H}_d = \sum_{j,\sigma}(\epsilon_d - \mu) d^\dagger_{j,\sigma} d_{j,\sigma} + U \sum_j n^\dagger_{j\uparrow} n_{j\downarrow} \\ -w \sum_{j,\sigma} [d^\dagger_{j+1,\sigma} d_{j,\sigma} + d^\dagger_{j,\sigma} d_{j+1,\sigma}], \tag{2}$$

and their hybridization with the superconductor,

$$\mathcal{H}_T = -t \sum_{j,\sigma} [\psi^\dagger_\sigma(\mathbf{R}_j) d_{j,\sigma} + d^\dagger_{j,\sigma} \psi_\sigma(\mathbf{R}_j)]. \tag{3}$$

Here, $d_{j,\sigma}$ annihilates a spin-σ electron in the d-level at site $\mathbf{R}_j = ja\hat{\mathbf{x}}$ of the chain, $n_{j,\sigma} = d^\dagger_{j,\sigma} d_{j,\sigma}$, and $\psi_\sigma(\mathbf{r})$ annihilates electrons at position $\mathbf{r}$ (taken as continuous) in the superconductor.

The model in Eq. (1) generalizes the Shiba chain model considered in [9] and [10]. It reduces to the Shiba chain in the limit of negligible spin fluctuations and weak intersite hopping w. Here, we include the hopping and the ensuing electronic dynamics of the magnetic adatoms within a mean-field treatment of the Hubbard term [37, 38],

$$U n^\dagger_{j\uparrow} n_{j\downarrow} \to \frac{U}{2} \sum_\sigma [\langle n_j \rangle n_{j,\sigma} + \langle m_j \rangle \sigma n_{j,\sigma}], \tag{4}$$

where we defined the occupation $n_j = \sum_\sigma n_{j,\sigma}$ and the site polarization $m_j = n_{j,\uparrow} - n_{j,\downarrow}$. The first term merely renormalizes ϵ_d and will be absorbed in the following. The second term introduces a local exchange coupling in the adatom orbitals.

As we are predominantly interested in the localization of the Majorana modes, we do not aim at a self-consistent solution of the mean-field theory. Instead, we accept the formation of a spontaneous moment as experimental fact and explore its consequences. In experiment, the moments order ferromagnetically along the chain. In this case, topological superconductivity requires the presence of Rashba spin-orbit coupling [26, 27]. For analytical tractability, we assume instead that the moments develop helical order $\mathbf{S}_j = (\sin\theta\cos\phi_j, \sin\theta\sin\phi_j, \cos\theta)$ with $\phi_j = 2k_h ja$ and $\theta = \pi/2$. We emphasize that the model with helical order can be mapped to a ferromagnetic model with spin-orbit coupling. Strictly speaking, the effective spin-orbit coupling generated by the mapping differs from conventional Rashba coupling, but it does include the specific term that allows for proximity-induced p-wave pairing. The mapping is effected by the unitary transformation $d_j \to e^{-ik_h ja\sigma_z} d_j$ and $\psi(\mathbf{r}) \to e^{-ik_h x\sigma_z}\psi(\mathbf{r})$ which rotates the spin basis along the direction of the local impurity moments [39, 40].

Excitation spectrum and phase diagram.—In mean-field theory, we can describe the system equivalently by the corresponding Bogoliubov-de Gennes Hamiltonian $H = H_d + H_s + H_T$ (after the above-mentioned unitary transformation) and consider the Green function $G = (E - H)^{-1}$. In view of the local nature of the hybridization H_T, we can write a closed set of equations for the restricted Green function $g_{ij} = G(\mathbf{R}_i, \mathbf{R}_j)$ defined at the sites of the adatoms,

$$\begin{pmatrix} (g_0^{\rm ss})^{-1} & t\tau_z \\ t\tau_z & E - H_d \end{pmatrix} g = 1. \tag{5}$$

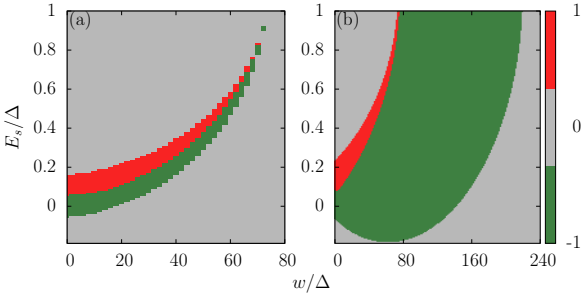

Figure 1. Representative phase diagrams for the adatom chain as a function of the Shiba state energy E_s of an individual impurity and the hopping amplitude w between d-levels. The colors indicate the topological index (grey: topologically trivial; red/green: topological phase with index ± 1). We chose $E_{d,\downarrow} = 100\Delta$, $k_F a = 4.3\pi$, $k_h = 0.26\pi$, and $\xi_0/a = \infty$. The panels correspond to (a) symmetric adatom d-bands ($E_{d,\uparrow} = -100\Delta$) and (b) asymmetric adatom d-bands ($E_{d,\uparrow} = -300\Delta$).

We use the Pauli matrices τ_i (σ_i) in particle-hole (spin) space. The bare Green function of the superconductor restricted to the adatom sites and subgap energies is readily obtained within BCS theory (see [40] for more details),

$$g^{\rm ss}_{0,ij}(E) = -\pi\nu_0 \exp(-ik_h x_{ij}\sigma_z) \times \left\{ \frac{E + \Delta\tau_x}{\sqrt{\Delta^2 - E^2}} \mathrm{Im} f(r_{ij}) + \tau_z \mathrm{Re} f(r_{ij}) \right\}, \tag{6}$$

where $f(r) = e^{ik_F r - r/\xi_E}/k_F r$ and $\xi_E = \hbar v_F/\sqrt{\Delta^2 - E^2}$. Eq. (6) is valid for $i \neq j$, but also applies to $i = j$ when dropping the Ref term. Here, the factor $\exp(-ik_h x_{ij}\sigma_z)$ is induced by the unitary transformation.

The subgap excitation spectrum may then be obtained from the poles of $g^{\rm ss} = g_0^{\rm ss}[1 - \Sigma g_0^{\rm ss}]^{-1}$ where we defined the self energy $\Sigma = t g_0^{\rm dd} t = t(E - H_d)^{-1} t$. As $g_0^{\rm ss}$ has no poles at subgap energies, this yields the condition $\det[1 - \Sigma g_0^{\rm ss}] = 0$. In (lattice) momentum representation, the determinant involves a 4×4 matrix with [40]

$$g_0^{\rm ss}(k, E) = \pi\nu_0 \left\{ \frac{E + \Delta\tau_x}{\sqrt{\Delta^2 - E^2}} L_i^{\sigma_z}(k, E) + \tau_z L_r^{\sigma_z}(k, E) \right\}. \tag{7}$$

Here, $L_r^{\sigma_z}$ and $L_i^{\sigma_z}$ are real and imaginary parts of the function $L^{\sigma_z} = F(k + k_h\sigma_z) - i$, respectively, with $F(k) = \frac{1}{k_F a} \ln\{1 - e^{i(k_F + k)a - a/\xi_E}\} + (k \leftrightarrow -k)$ [41]. Computing the dispersions and identifying phase boundaries by the closing of the gap, we first obtain representative phase diagrams of the adatom chain as shown in Fig. 1.

These phase diagrams make the interpolation between the band and Shiba limits explicit. The Shiba limit corresponds to weak hopping w between d-levels, while the band limit corresponds to weak hybridization $\Gamma = \pi\nu_0 t^2$ and thus Shiba states with energies near Δ [38]. The existence of phases with (BDI [42]) topological indices ± 1, known for the Shiba chain, persists in the band limit.

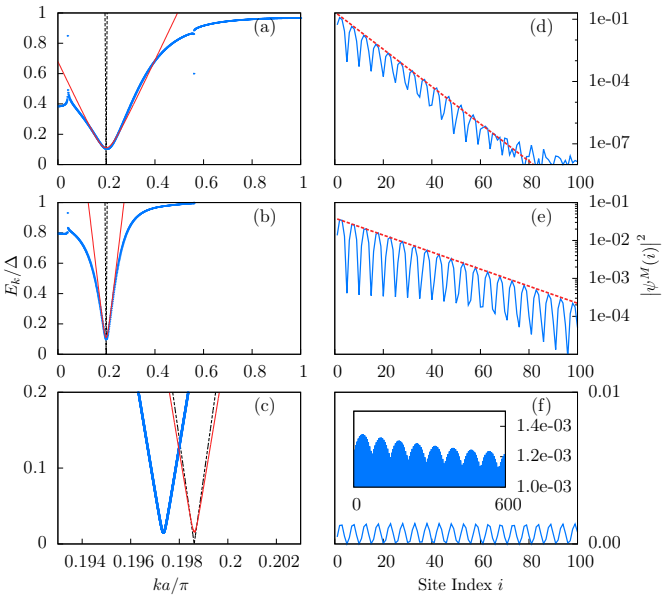

Figure 2. Excitation spectra E_k for $ka/\pi \in [0,1]$ and (a) $\Gamma = 64\Delta$, (b) $\Gamma = 16\Delta$, and (c) $\Gamma = 0.16\Delta$. We chose $k_F a = 4.3\pi$, $k_h a = 0.26\pi$, $E_{d,\downarrow} = 100\Delta$, $E_{d,\uparrow} = -19900\Delta$, $w = 90\Delta$, and $\xi_0/a = \infty$. The dashed lines are subgap dispersions of the impurity chain without coupling to the superconductor. The blue curves are exact dispersions. The red curves are calculated using Eq. (11) for $\Gamma \gg \Delta$ and (10) for $\Gamma \ll \Delta$. Notice that the horizontal axis in (c) is restricted to a very narrow range and that the deviation between the red and blue curves is indeed small. Panels (d), (e), and (f) show Majorana wavefunctions $|\psi^M(i)|^2$ (blue lines) obtained for a finite chain of length $L = 1500a$. Only the first 100 sites i are shown. (d) and (e) are plotted on a logarithmic scale and the red dashed lines are fits using Eq. (12) for the Majorana localization length. (f) is plotted on a linear scale. Inset: Decay over the first 600 sites.

The two phase diagrams in Fig. 1 differ in the asymmetry of the bare exchange-split adatom states $E_{d,\sigma} = \epsilon_d - \sigma U\langle m\rangle/2$ about the Fermi energy (set to $\mu = 0$). Fig. 1(a) shows the symmetric case $E_{d,\uparrow} = -E_{d,\downarrow}$. There is only a narrow topological interval in w for small Γ ($E_s \simeq \Delta$). This is easily understood because despite the large exchange splitting of the d-levels, the spin-split d-bands cross the Fermi energy at the same hopping strength w. As the asymmetry between $E_{d,\uparrow}$ and $E_{d,\downarrow}$ about the Fermi energy increases, the d-bands cross the Fermi energy at different values of w, and there is a substantial region in which the adatom states at the Fermi energy are perfectly spin-polarized, cf. Fig. 1(b). The asymmetry also affects the Shiba limit at small w as it introduces potential scattering into the effective Hamiltonian, in addition to the exchange coupling.

For fully analytical results, we consider the limit of strong asymmetry with $E_{d,\uparrow} \to -\infty$ at fixed $E_{d,\downarrow}$. In this limit, only the spin-down band $E_d = E_{d,\downarrow} - w\sum_{\pm}\cos(k \pm k_h)a$ of the d-levels is relevant and the self energy Σ simplifies to [40]

$$\Sigma = e^{i\frac{\pi}{4}\sigma_y}\left[\frac{\alpha_-}{\pi\nu_0}\frac{1+\tau_z}{2} + \frac{\alpha_+}{\pi\nu_0}\frac{1-\tau_z}{2}\right](\sigma_z - \tau_z)e^{-i\frac{\pi}{4}\sigma_y} \tag{8}$$

in terms of the dimensionless quantities $\alpha_\pm = \Gamma/(2E_d \pm 2E)$ with $\Gamma = \pi\nu_0 t^2$. Note that $\alpha_\pm$ still depends on the energy E of the excitation. A detailed but straightforward calculation [40] now shows that the condition $\det(1 - \Sigma g_0^{ss}) = 0$ can be reduced to the determinant of a 2×2-matrix and written in the form

$$(\Delta^2 - E^2)[E_d + \Gamma L_r]^2 - E^2[\sqrt{\Delta^2 - E^2} - \Gamma L_i]^2 + \Gamma^2\Delta^2(\delta L_i)^2 = 0. \tag{9}$$

Here, we introduced the shorthand notations $L_{r/i} = (L^+_{r/i} + L^-_{r,i})/2$ and $\delta L_i = (L^+_i - L^-_i)/2$. Eq. (9) is an implicit equation for the subgap excitation spectrum E_k of the adatom chain in the strongly asymmtric limit. [Note that we have suppressed all k labels in Eq. (9).]

We first discuss the predictions of Eq. (9) for the excitation spectrum. Explicit analytical expressions valid throughout the entire Brillouin zone are easily obtained from Eq. (9) in the limits $\Gamma \ll \Delta$ and $\Gamma \gg \Delta$. Keeping only the respective dominant term in the square brackets of the second term of the left hand side yields expressions which are in excellent agreement with the solution of Eq. (9) in Fig. 2(a)-(c). We note that within mean-field theory, there is a single subgap state for every lattice momentum k, i.e., there is one subgap state per adatom of the chain, as in the Shiba limit (small w).

Majorana wavefunction.—Eq. (9) also encapsulates essential information on the localization of the Majorana wavefunctions. In the Shiba limit of small w, the localization of the Majorana wavefunctions was addressed previously [43]. Here, we focus on the band limit of large w in which the d-bands can cross the Fermi energy of the superconductor, as is presumably the case in the experiment [26, 27]. In this limit, the spin-down band E_d crosses $\mu = 0$ at momenta k_0. In the vicinity of k_0, we can approximate $E_d \simeq v_F(k - k_0)$, where v_F is the Fermi velocity of the d-band at the chemical potential of the superconductor. Similarly, $E_d + \Gamma L_r \simeq v_F(k - k_0)$ where we simply absorb the parametrically small shifts in v_F and k_0 due to ΓL_r into their definitions.

We expect that the decay of the Majorana wavefunction is controlled by the behavior of the dispersion near the minimal gap at the k_0. Assuming that the pitch of the spin helix (or, equivalently, the strength of the spin-orbit coupling) is not too large, the minimal gap will be small compared to the gap Δ of the superconducting host. Then, E is small compared to Δ in the relevant region and Eq. (9) simplifies significantly. Consider first the limit of weak hybridization $\Gamma \ll \Delta$. In this limit, Eq. (9) reduces to

$$E_k = \pm\sqrt{[v_F(k - k_0)]^2 + \Gamma^2(\delta L_i)^2}, \tag{10}$$

where δL_i should be evaluated at k_0. We identify the induced gap $\Delta_{\rm ind} = \Gamma(\delta L_i)_{k=k_0}$ which is small compared to Δ. We note in passing that this gap is enabled by the (effective) spin-orbit interaction in the superconductor, cp. [44, 45]). The Majorana wavefunction is expected to decay on the characteristic length scale of this dispersion, i.e., we find the Majorana localization length $\xi_M = \hbar v_F/\Delta_{\rm ind}$. This is larger than the coherence length of the host superconductor (assuming a bandwidth of the adatom d-band on atomic scales so that v_F is comparable to the host Fermi velocity). For the numerical parameters of Fig. 2(c), ξ_M is larger than the length of the chain, making a direct comparison impossible.

The experiment is in the limit of large hybridization $\Gamma \gg \Delta$, where Eq. (9) predicts a low-energy dispersion

$$E_k = \pm\sqrt{[(\Delta/\Gamma L_i)v_F(k-k_0)]^2 + [\Delta(\delta L_i/L_i)]^2}. \quad (11)$$

In this limit, the induced gap $\Delta_{\rm ind} = \Delta(\delta L_i/L_i)_{k=k_0}$ is independent of Γ and saturates to a value which is smaller than Δ by a factor measuring the strength of the (effective) spin-orbit coupling. The strong hybridization with the superconductor also induces a dramatic downward renormalization of the Fermi velocity of the excitations, $v_F \to \tilde{v}_F = (\Delta/\Gamma L_i)v_F$. Both features are in excellent agreement with the numerical subgap spectra as shown in Figs. 2(a) and (b).

Eq. (11) predicts a Majorana localization length $\xi_M = \hbar\tilde{v}_F/\Delta_{\rm ind}$. Thus, we find

$$\xi_M = \frac{\hbar v_F}{\Gamma(\delta L_i)} \quad (12)$$

when $\Gamma \gg \Delta$. (This expression actually also holds in the opposite limit $\Gamma \ll \Delta$.) We see that ξ_M is independent of the host gap Δ and controlled by the hybridization Γ. This result is in excellent agreement with numerical calculations of the Majorana wavefunctions for $\Gamma \gg \Delta$, see Figs. 2(d) and (e). Importantly, in the limit $\Gamma \gg \Delta$, ξ_M is smaller by a factor $\Delta/(\Gamma\delta L_i)$ than the coherence length ξ_0 of the host superconductor ($\xi_0 \simeq 100$nm for Pb). We estimate $\xi_M \sim \xi_0(\Delta/\Gamma)(\Delta/\Delta_{\rm ind})$. In experiment, the hybridization Γ is controlled by atomic scales and should thus be of order 1eV which is about three orders of magnitudes larger than the host gap $\Delta \sim 10$K. For $\Delta_{\rm ind}/\Delta \sim 0.1$, the Majorana localization length ξ_M becomes of the order of the spacing between adatoms.

The hybridization of the d-levels with the host superconductor results in a transfer of the spectral weight of the subgap excitations to the host, similar to an observation made in the context of 3D hybrid systems [46]. The velocity renormalization $v_F \to \tilde{v}_F = (\Delta/\Gamma L_i)v_F$ evident in Eq. (11) is a consequence of that transfer. The fraction of time an excitation spends in the band is suppressed by a factor $\Delta/\Gamma \ll 1$, which results in a reduced effective velocity $\tilde{v}_F$. (This is opposite to the quantum-wire setting, where this renormalization is usually assumed to be small, see, e.g., [47].) The in-band propagation between adjacent sites takes time $\tau \sim a/\tilde{v}_F$. As long as τ is shorter than the time $(\Delta L_r)^{-1}$ for hopping via the host superconductor [10], the spectrum Eq. (11) remains a good approximation. That imposes the condition $\Gamma \ll v_F/a$ for the validity of Eqs. (11) and (12). Besides the minimum described by Eq. (11), the quasiparticle spectrum has additional features associated with logarithmic divergencies in L_r. They induce power-law tails in the Majorana wavefunctions which become correspondingly more pronounced as Γ increases.

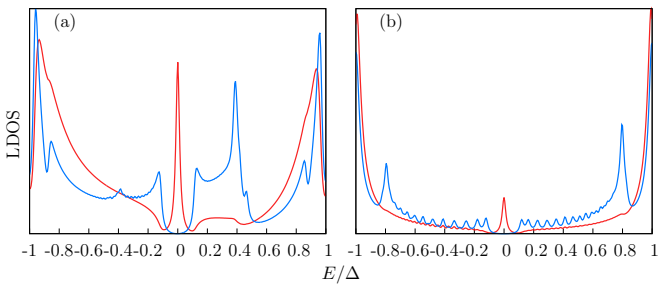

Figure 3. Local density of states of particle excitations, computed in the center (blue) and at the end (red), for a chain of length $L = 300a$ and hybridizations (a) $\Gamma = 64$ and (b) $\Gamma = 16$. Other parameters are as in Fig. 2.

Local density of states.—We have also numerically computed [40] the local density of states of the adatom chain within the mean-field approximation, see Fig. 3. In addition to the zero-energy Majorana peak, one discerns additional peaks at finite energies which arise from van Hove singularities in the subgap Shiba band. These peaks approach the center of the gap as the hybridization Γ increases and are reminiscent of similar peaks in the experiment [26]. Note also that the zero-bias peak grows more pronounced with increasing Γ, reflecting the stronger localization of the Majorana wavefunction.

Conclusions.—Motivated by a recent experiment [26], we analyze a chain of Anderson impurities in a host superconductor by largely analytical means. We find a topological superconducting phase characterized by the presence of strongly localized zero-energy Majorana states and additional Shiba subgap peaks. The corresponding features in the local density of states bear strong similarity to those observed in experiment [26].

Acknowledgments.— We thank Ali Yazdani, Andrei Bernevig, Titus Neupert, Piet Brouwer, and Allan MacDonald for stimulating discussions. We acknowledge financial support by the Helmholtz Virtual Institute "New states of matter and their excitations," SPP1285 and SPP1666 of the Deutsche Forschungsgemeinschaft, the Humboldt Foundation, NSF DMR Grant 1206612, and ONR Grant Q00704. We are grateful to the Aspen Center for Physics, supported by NSF Grant No. PHYS-106629, for hospitality while this line of work was initiated.

[1] J. Alicea, Rep. Prog. Phys. **75**, 076501 (2012).
[2] C.W.J. Beenakker, Annu. Rev. Con. Mat. Phys. **4**, 113 (2013).
[3] A. Kitaev, Ann. Phys. **303**, 2 (2003).
[4] L. Fu and C.L. Kane, Phys. Rev. Lett. **100**, 096407 (2008).
[5] L. Fu and C. L. Kane, Phys. Rev. B **79**, 161408(R) (2009).
[6] R.M. Lutchyn, J.D. Sau, and S. Das Sarma, Phys. Rev. Lett. **105**, 077001 (2010).
[7] Y. Oreg, G. Refael, and F. von Oppen, Phys. Rev. Lett. **105**, 177002 (2010).
[8] J. Alicea, Y. Oreg, G. Refael, F. von Oppen, and M.P.A. Fisher, Nature Phys. **7**, 412 (2011).
[9] S. Nadj-Perge, I.K. Drozdov, B.A. Bernevig, and A. Yazdani, Phys. Rev. B **88**, 020407(R) (2013).
[10] F. Pientka, L.I. Glazman, and F. von Oppen, Phys. Rev. B **88**, 155420 (2013).
[11] Y. Kim, M. Cheng, B. Bauer, R.M. Lutchyn, and S. Das Sarma, Phys. Rev. B **90**, 060401(R) (2014)
[12] J. Klinovaja, P. Stano, A. Yazdani, and D. Loss, Phys. Rev. Lett. **111**, 186805 (2013).
[13] B. Braunecker and P. Simon, Phys. Rev. Lett. **111**, 147202 (2013).
[14] M.M. Vazifeh and M. Franz, Phys. Rev. Lett. **111**, 206802 (2013).
[15] T.-P. Choy, J.M. Edge, A.R. Akhmerov, and C.W.J. Beenakker, Phys. Rev. B **84**, 195442 (2011).
[16] M. Kjaergaard, K. Wï¿œlms, and K. Flensberg, Phys. Rev. B **85**, 020503 (2012).
[17] I. Martin, and A. Morpurgo, Phys. Rev. B **85**, 144505 (2012).
[18] V. Mourik, K. Zuo, S.M. Frolov, S.R. Plissard, E.P.A.M. Bakkers, and L.P. Kouwenhoven, Science **336**, 1003 (2012).
[19] A. Das, Y. Ronen, Y. Most, Y. Oreg, M. Heiblum, and H. Shtrikman, Nature Phys. **8**, 887 (2012).
[20] H.O.H. Churchill, V. Fatemi, K. Grove-Rasmussen, M.T. Deng, P. Caroff, H.Q. Xu, and C.M. Marcus, Phys. Rev. B **87**, 241401(R) (2013).
[21] L.P. Rokhinson, X. Liu, and J.K. Furdyna, Nature Phys. **8**, 795 (2012).
[22] M.T. Deng, C.L. Yu, G.Y. Huang, M. Larsson, P. Caroff, and H.Q. Xu, Nano Lett. **12**, 6414 (2012).
[23] A.D.K. Finck, D.J. Van Harlingen, P.K. Mohseni, K. Jung, and X. Li, Phys. Rev. Lett. **110**, 126406 (2013).
[24] S. Hart, H. Ren, T. Wagner, P. Leubner, M. Mühlbauer, C. Brüne, H. Buhmann, L.W. Molenkamp, and A. Yacoby, Nature Phys. **10**, 638 (2014).
[25] V.S. Pribiag, A.J.A. Beukman, F. Qu, M.C. Cassidy, C. Charpentier, W. Wegscheider, and L.P. Kouwenhoven, arXiv:1408.1701 (2014).
[26] S. Nadj-Perge, I.K. Drozdov, J. Li, H. Chen, S. Jeon, J. Seo, A.H. MacDonald, B.A. Bernevig, A. Yazdani, Science Science **346**, 602 (2014).
[27] J. Li, H. Chen, I.K. Drozdov, A. Yazdani, B.A. Bernevig, A.H. MacDonald, arXiv:1410.3453 (2014).
[28] E. Dumitrescu, B. Roberts, S. Tewari, J.D. Sau, S. Das Sarma, arXiv:1410.5412 (2014).
[29] P.A. Lee, Commentary on Ref. [26], Journal Club for Condensed Matter Physics, http://www.condmatjournalclub.org/?m=201410.
[30] S. Nakosai, Y. Tanaka, and N. Nagaosa, Phys. Rev. B **88**, 180503(R) (2013).
[31] K. Pöyhönen, A. Weststrom, J. Röntynen, and T. Ojanen, Phys. Rev. B **89**, 115109 (2014).
[32] A. Heimes, P. Kotetes, G. Schön, Phys. Rev. B **90**, 060507(R) (2014).
[33] L. Yu, Acta Phys. Sin. **21**, 75 (1965).
[34] H. Shiba, Prog. Theor. Phys. **40**, 435 (1968).
[35] A.I. Rusinov, Zh. Eksp. Teor. Fiz. Pisma Red. **9**, 146 (1968) [JETP Lett. **9**, 85 (1969)].
[36] A.V. Balatsky, I. Vekhter, and J.-X. Zhu, Rev. Mod. Phys. **78**, 373 (2006).
[37] P.W. Anderson, Phys. Rev. **124**, 41 (1961).
[38] H. Shiba, Prog. Theor. Phys. **50**, 50 (1973).
[39] B. Braunecker, G.I. Japaridze, J. Klinovaja, and D. Loss, Phys. Rev. B **82**, 045127 (2010).
[40] Supplementary Material
[41] The function L is plotted in [40]. Roughly, $L_i^{\sigma_z}$ (and hence L_i) is of order unity. $L_r^{\sigma_z}$ (and hence L_r) is of order $1/k_F a$, except at isolated values of k where it has logarithmic singularities. δL_i should be thought of as a dimensionless measure of the effective spin-orbit strength, which is also of order $1/k_F a$ for our spin-helix model.
[42] S. Ryu, A.P. Schnyder, A. Furusaki, and A.W.W. Ludwig, New J. Phys. **12**, 065010 (2010).
[43] F. Pientka, L.I. Glazman, and F. von Oppen, Phys. Rev. B **89**, 180505(R) (2014).
[44] M. Duckheim, P.W. Brouwer, Phys. Rev. B **83**, 054513 (2011).
[45] S.B. Chung, H.J. Zhang, X.L. Qi, S.C. Zhang, Phys. Rev. B **84**, 060510(R) (2011).
[46] A.C. Potter and P.A. Lee, Phys. Rev. B **83**, 184520 (2011).
[47] A.A. Zyuzin, S. Rainis, J. Klinovaja, and D. Loss, Phys. Rev. Lett. **111**, 056802 (2013).

SUPPLEMENTARY MATERIAL

I. UNITARY TRANSFORMATION OF HAMILTONIAN WITH HELICAL ORDER

The mean-field Hamiltonian for a chain of Anderson impurities coupled to an s-wave superconductor can be written as

$$\mathcal{H} = \mathcal{H}_s + \mathcal{H}_d + \mathcal{H}_T, \tag{1}$$

with

$$\mathcal{H}_d = \sum_{j,\sigma}(\epsilon_d - \mu)\tilde{d}^\dagger_{j,\sigma}\tilde{d}_{j,\sigma} - w\sum_{j,\sigma}\left(\tilde{d}^\dagger_{j,\sigma}\tilde{d}_{j+1,\sigma} + \tilde{d}^\dagger_{j+1,\sigma}\tilde{d}_{j,\sigma}\right) - K\sum_{j,\sigma,\sigma'}\mathbf{S}_j\tilde{d}^\dagger_{j,\sigma}\boldsymbol{\sigma}_{\sigma,\sigma'}\tilde{d}_{j,\sigma'}, \tag{2}$$

where the exchange term $K|\mathbf{S}_j| = U/2$ arises from a mean-field treatment of the local Hubbard interaction as described in the main text. Using the Nambu spinor notation $\tilde{d}_j = (\tilde{d}_{j\uparrow}, \tilde{d}_{j\downarrow}, \tilde{d}^\dagger_{j\downarrow}, -\tilde{d}^\dagger_{j\uparrow})^T$, we can write down its Bogoliubov-de Gennes Hamiltonian

$$\mathcal{H}_d = \frac{1}{2}\sum_{ij}\tilde{d}^\dagger_i\tilde{H}^{ij}_d\tilde{d}_j \tag{3}$$

$$\tilde{H}^{ij}_d = \left[(\epsilon_d - \mu)\tau_z - K\mathbf{S}_j\cdot\boldsymbol{\sigma}\right]\delta_{ij} - w\tau_z(\delta_{i,j-1} + \delta_{i,j+1}), \tag{4}$$

where the τ_i with $i = x, y, z$ are Pauli matrices in particle-hole space. The s-wave superconductor is modeled by the BCS Hamiltonian

$$\mathcal{H}_s = \frac{1}{2}\int d^3r\,\tilde{\psi}^\dagger(\mathbf{r})\tilde{H}_s\tilde{\psi}(\mathbf{r}) \tag{5}$$

$$\tilde{H}_s = \xi_{\mathbf{p}}\tau_z + \Delta\tau_x \tag{6}$$

$$\xi_{\mathbf{p}} = \frac{\mathbf{p}^2}{2m} - \mu, \tag{7}$$

where $\tilde{\psi}(\mathbf{r}) = (\tilde{\psi}_\uparrow(\mathbf{r}), \tilde{\psi}_\downarrow(\mathbf{r}), \tilde{\psi}^\dagger_\downarrow(\mathbf{r}), -\tilde{\psi}^\dagger_\uparrow(\mathbf{r}))^T$, and Δ is the superconducting order parameter. The hybridization between the magnetic adatoms and the superconductor in particle-hole space is given by

$$\mathcal{H}_T = -\frac{t}{2}\sum_j\left(\tilde{\psi}^\dagger(\mathbf{R}_j)\tau_z\tilde{d}_j + h.c.\right), \tag{8}$$

where $\mathbf{R}_j = ja\hat{\mathbf{x}}$ denotes the position of the jth magnetic adatom, t the hybridization strength, and a the lattice spacing along the chain (i.e., the x) direction.

We assume a spin helix configuration

$$\mathbf{S}_j = (\sin\theta_j\cos\phi_j, \sin\theta_j\sin\phi_j, \cos\theta_j) \tag{9}$$

with $\theta_j = \theta$ and $\phi_j = 2k_hja$, i.e., the spin rotates about the z-axis with wavevector $2k_h$ and opening angle θ. This is equivalent to a ferromagnetic configuration with a particular type of spin-orbit coupling via a unitary transformation. Explicitly, we transform $\psi(\mathbf{r}) = e^{ik_hx\sigma_z}\tilde{\psi}(\mathbf{r})$ and $d_j = e^{ik_hja\sigma_z}\tilde{d}_j$, which rotates the local spin quantization axis along the local direction of the magnetic moment, or equivalently, maps the system on a ferromagnetic configuration. For the superconductor, this yields

$$\mathcal{H}_s = \frac{1}{2}\int d^3r\psi^\dagger(\mathbf{r})H_s\psi(\mathbf{r}) \tag{10}$$

$$H_s = \left[\frac{(\mathbf{p} + k_h\sigma_z\hat{x})^2}{2m}\right]\tau_z + \Delta\tau_x. \tag{11}$$

The Hamiltonian for the chain of magnetic adatoms transforms into

$$\mathcal{H}_d = \frac{1}{2}\sum_{ij}d^\dagger_iH^{ij}_dd_j \tag{12}$$

$$H^{ij}_d = \left[(\epsilon_d - \mu)\delta_{ij} - W_{ij}\right]\tau_z - K\mathbf{S}\cdot\boldsymbol{\sigma}\delta_{ij} \tag{13}$$

with $W_{ij} = -we^{-ik_h a\sigma_z}$ if $i = j+1$, $W_{ij} = -we^{ik_h a\sigma_z}$ if $i = j-1$, and zero otherwise. Finally we have the hybridization term

$$\mathcal{H}_t = -\frac{t}{2}\sum_j \left(\psi^\dagger(\mathbf{R}_j)\tau_z d_j + h.c.\right), \tag{14}$$

which is invariant under this transformation.

We observe that in the transformed Hamiltonian, the helix wavevector plays the role of the strength of (a particular type of) spin-orbit coupling. There is spin-orbit coupling in both the wire and the superconductor. It can be seen from the results of the main text that it is predominantly the spin-orbit coupling in the superconductor that is operative in inducing a p-wave gap in the excitation spectrum. This is true as long as the exchange splitting of the d-bands is large compared to the effective spin-orbit strength.

The angle between the exchange splitting and the spin-orbit field depends on the opening angle θ of the spin helix. The optimal situation for topological superconductivity is when exchange splitting and spin-orbit field are orthogonal to one another. This happens for a planar spin helix $\theta = \pi/2$ which is what we consider in the main text and in the following. Explicitly, for this choice the exchange field is along the x-direction, $K\mathbf{S}\cdot\boldsymbol{\sigma} = KS\sigma_x$, with $S = |\mathbf{S}|$, while the spin-orbit field is along the z-direction.

Note that the spin-orbit coupling contains only the momentum along the chain. This is different from a conventional Rashba coupling where momenta along both directions of the surface would appear. Presumably, this has mostly quantitative consequences as it is the momentum along the chain which is essential for allowing induced p-wave pairing in the adatom band.

We finally note that one may also want to include pairing correlations $\langle d_{i\uparrow} d_{j\downarrow}\rangle$ in the mean field approximation for the Hubbard interaction on the adatom sites. We have neglected them as we assume a large exchange splitting of the d-bands which should strongly suppress any influence of these additional pairing correlations.

II. DERIVATION OF THE LATTICE GREEN FUNCTION

We write the Hamiltonian of the total system as

$$H = \begin{pmatrix} H_s & H_t \\ H_t^\dagger & H_d \end{pmatrix} = H_0 + H_T, \tag{15}$$

where H_s and H_d were defined in Eqs. (11) and (13), $H_0 = \mathrm{diag}(H_s, H_d)$ contains the diagonal terms, and H_T describes the hybridization on the off-diagonal

$$H_t^{\mathbf{r},j} = -t\delta(\mathbf{r} - \mathbf{R}_j)\tau_z. \tag{16}$$

Define the wavefunction of the composite system to be $\boldsymbol{\Psi} = (\boldsymbol{\psi}, \mathbf{d})^T$, where the two components will be referred as s and d components (which are still vectors) in the following. Then the Schrödinger equation can be written as

$$\sum_J H_{IJ}\Psi_J = E\Psi_I. \tag{17}$$

Here the indices I, J can be continuous coordinates $\mathbf{r} \in \mathbb{R}^3$ labeling the s components or be discrete $j \in \mathbb{Z}$ labeling the d components, and the summation over J combines the integration over continuous position and the summation over the discrete site index. Plugging Eq. (11), (13), (16) into the Schrödinger equation, we have

$$\left\{\left[\frac{(-i\partial_{\mathbf{r}} + k_h\sigma_z\hat{x})^2}{2m}\right]\tau_z + \Delta\tau_x\right\}\psi(\mathbf{r}) - t\sum_j \delta(\mathbf{r} - \mathbf{R}_j)\tau_z d_j = E\psi(\mathbf{r}) \tag{18}$$

$$-t\int dr^3\, \delta(\mathbf{r} - \mathbf{R}_i)\tau_z\psi(\mathbf{r}) + \sum_j \left\{\left[(\epsilon_d - \mu)\delta_{ij} - W_{ij}\right]\tau_z - K\mathbf{S}\cdot\boldsymbol{\sigma}\delta_{ij}\right\} d_j = E d_i. \tag{19}$$

The normalization condition is given by

$$\int d^3r\, \psi(r)^\dagger\psi(r) + \sum_j d_j^\dagger d_j = 1. \tag{20}$$

Notice that the s components $\psi(r)$ have units of [volume]$^{-1/2}$ while the d components are dimensionless.

Now we turn to the Green function of the system, which reads

$$G(E) = (E-H)^{-1} = (E-H_0-H_T)^{-1} = G_0(E) + G_0(E)H_T G_0(E) + G_0(E)H_T G_0(E)H_T G_0(E) + \cdots, \tag{21}$$

where $G_0(E) = (E-H_0)^{-1}$. Let us now define a reduced Green function g in which we restrict the position arguments of the superconductor to the discrete impurity sites. For instance, in the ss block, this reduced lattice Green function is defined as $g^{ss}_{ij} = G^{ss}(\mathbf{R}_i, \mathbf{R}_j)$ with $i, j \in \mathbb{Z}$ (as opposed to $G^{ss}(\mathbf{R}_i, \mathbf{R}_j)$ with $\mathbf{R}_i, \mathbf{R}_j \in \mathbb{R}^3$). Let's compute the separate blocks of g in (s,d) space (space formed by superconductor and d levels of Anderson impurities),

$$g^{dd}_{ij} = g^{dd}_{0,ij} + \sum_{k_1 k_2} g^{dd}_{0,ik_1}(-t\tau_z) g^{ss}_{0,k_1k_2}(-t\tau_z) g^{dd}_{0,k_2 j} + \cdots \tag{22}$$

$$g^{ss}_{ij} = g^{ss}_{0,ij} + \sum_{k_1 k_2} g^{ss}_{0,ik_1}(-t\tau_z) g^{dd}_{0,k_1k_2}(-t\tau_z) g^{ss}_{0,k_2 j} + \cdots \tag{23}$$

$$g^{ds}_{ij} = \sum_{k_1} g^{dd}_{0,ik_1}(-t\tau_z) g^{ss}_{0,k_1 j} + \cdots. \tag{24}$$

with the notation

$$g^{ss}_{0,ij} = G^{ss}_0(\mathbf{R}_i, \mathbf{R}_j), \qquad g^{ds}_{0,ij} = G^{ds}_0(i, \mathbf{R}_j). \tag{25}$$

We obtain the inverse of the lattice Green function, in matrix notation,

$$g^{-1} = \begin{pmatrix} (g^{ss}_0)^{-1} & t\tau_z \\ t\tau_z & E - H_d \end{pmatrix}, \tag{26}$$

leading to Eq. (5) of the main text. Here, g^{-1} is a matrix in (s,d) space, in site space, and in spin and particle-hole space. (The spin and particle-hole indices are implicitly included in the site labels.)

We first compute the Green function of the superconductor. For $i \neq j$,

$$\begin{aligned}
g^{ss}_{0,ij}(E) &= \langle \mathbf{R}_i | \, (E - H_s)^{-1} \, | \mathbf{R}_j \rangle \\
&= \langle \mathbf{R}_i | \left[E - \left(\frac{(\mathbf{p} + k_h a \sigma_z \hat{x})^2}{2m} - \mu \right) \tau_z - \Delta \tau_x \right]^{-1} | \mathbf{R}_j \rangle \\
&= \langle \mathbf{R}_i | \, e^{-ik_h x \sigma_z} \left[E - \left(\frac{(\mathbf{p} + k_h a \sigma_z \hat{x})^2}{2m} - \mu \right) \tau_z - \Delta \tau_x \right]^{-1} e^{ik_h x \sigma_z} \, | \mathbf{R}_j \rangle \\
&= e^{-ik_h (i-j) a \sigma_z} \frac{1}{V} \sum_{\mathbf{k}} \frac{e^{i\mathbf{k}\cdot(\mathbf{R}_i - \mathbf{R}_j)}}{E - \xi_k \tau_z - \Delta \tau_x} \\
&= e^{-ik_h (i-j) a \sigma_z} \left[(E + \Delta\tau_x) P_0(|i-j| \, a) + \tau_z P_1(|i-j| \, a) \right]
\end{aligned}$$

where [10]

$$P_0(r) = \frac{\nu_0}{2} \int d\xi_k \int_{-1}^{1} dx \, \frac{e^{ikrx}}{E^2 - \xi_k^2 - \Delta^2} = -\frac{\pi \nu_0}{\sqrt{\Delta^2 - E^2}} \frac{\sin k_F r}{k_F r} e^{-r/\xi_E} \tag{27}$$

$$P_1(r) = \frac{\nu_0}{2} \lim_{\omega_D \to \infty} \int d\xi_k \int_{-1}^{1} dx \, \frac{\xi_k e^{ikrx}}{E^2 - \xi_k^2 - \Delta^2} \frac{\omega_D^2}{\xi_k^2 + \omega_D^2} = -\pi \nu_0 \frac{\cos k_F r}{k_F r} e^{-r/\xi_E} \tag{28}$$

with ν_0 the normal density of states at the Fermi energy and $\xi_E = v_F/\sqrt{\Delta^2 - E^2}$. Then we obtain

$$g^{ss}_{0,ij}(E) = -\pi \nu_0 e^{-ik_h x_{ij} \sigma_z} \left\{ \frac{E + \Delta\tau_x}{\sqrt{\Delta^2 - E^2}} \frac{\sin k_F r_{ij}}{k_F r_{ij}} e^{-r_{ij}/\xi_E} + \tau_z \frac{\cos k_F r_{ij}}{k_F r_{ij}} e^{-r_{ij}/\xi_E} \right\} \tag{29}$$

where $x_{ij} = x_i - x_j = (i-j)a$, $r_{ij} = |x_{ij}|$. We can also rewrite it as

$$g^{ss}_{0,ij}(E) = -\pi \nu_0 e^{-ik_h x_{ij} \sigma_z} \left\{ \frac{E + \Delta\tau_x}{\sqrt{\Delta^2 - E^2}} \mathrm{Im} f(r_{ij}) + \tau_z \mathrm{Re} f(r_{ij}) \right\} \tag{30}$$

with

$$f(r) = \frac{e^{ik_F r - r/\xi_E}}{k_F r}. \tag{31}$$

For $i = j$, we find (see Ref. [10] for details)

$$g^{ss}_{0,ii}(E) = -\pi\nu_0 \frac{E + \Delta\tau_x}{\sqrt{\Delta^2 - E^2}}. \tag{32}$$

III. GREEN FUNCTION IN LATTICE MOMENTUM SPACE

We proceed by computing the Green function in lattice momentum space

$$g^{ss}_0(k) = \sum_j e^{-ikx_{ij}} g^{ss}_{0,ij} = g^{ss}_{0,ii} + 2\sum_{j=1}^{\infty} \cos((k + k_h\sigma_z)ja)\tilde{g}^{ss}_{0j}, \tag{33}$$

where

$$\tilde{g}^{ss}_{ij} = -\pi\nu_0 \frac{E + \Delta\tau_x}{\sqrt{\Delta^2 - E^2}} \mathrm{Im} f(r_{ij}) - \pi\nu_0\tau_z \mathrm{Re} f(r_{ij}). \tag{34}$$

For convenience, we define

$$F(k) = -2\sum_{j=1}^{\infty} \cos(k_F ja) f(ja) \tag{35}$$

$$= \frac{1}{k_F a}\left[\ln(1 - e^{-a/\xi_E + i(k_F + k)a}) + \ln(1 - e^{-a/\xi_E + i(k_F - k)a})\right], \tag{36}$$

which has the property $F(k) = F(-k)$, and define $L^{\sigma_z}(k) = F(k + k_h\sigma_z) - i$. We then obtain the Green function in lattice momentum space

$$g^{ss}_0(k) = \frac{\pi\nu_0(E + \Delta\tau_x)}{\sqrt{\Delta^2 - E^2}} L^{\sigma_z}_i(k, E) + \pi\nu_0\tau_z L^{\sigma_z}_r(k, E) \tag{37}$$

where $L^{\sigma_z}_i$ and $L^{\sigma_z}_r$ are the imaginary and real parts of L^{σ_z}, cf. Eq. (7) of the main text.

IV. NUMERICAL CALCULATION OF PHYSICAL QUANTITIES

A. Excitation spectrum

The inverse Green function g^{-1} is diagonal in momentum space and we have

$$g^{-1}(k, E) = \begin{pmatrix} (g^{ss}_0)^{-1}(k, E) & t\tau_z \\ t\tau_z & (g^{dd}_0)^{-1}(k, E) \end{pmatrix}, \tag{38}$$

with

$$(g^{dd}_0)^{-1}(k, E) = E - [\epsilon_d - 2w\cos(k + k_h\sigma_z)]\tau_z + KS\sigma_x. \tag{39}$$

This is an 8×8 matrix as a function of $k \in [-\frac{\pi}{a}, \frac{\pi}{a}]$. Then the subgap band can be calculated by imposing the condition

$$\det(g^{-1}(k, E)) = 0. \tag{40}$$

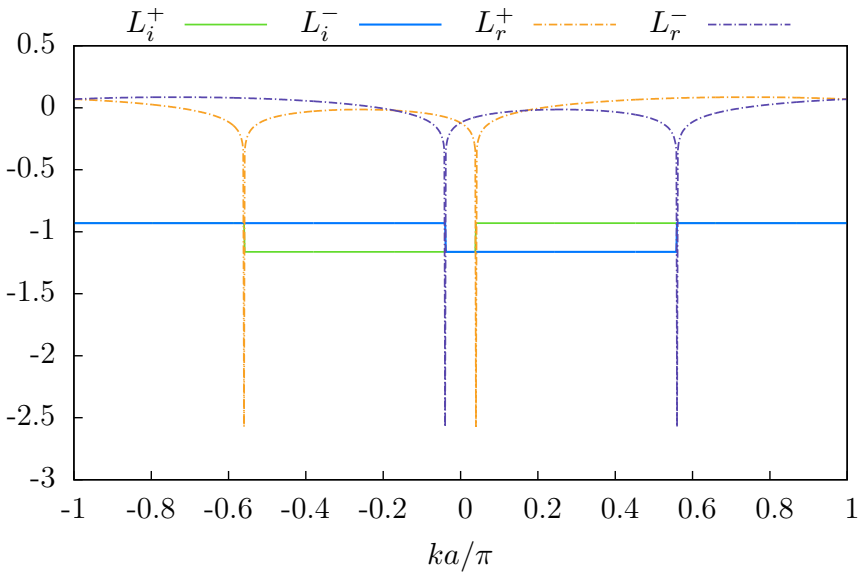

Figure 4. $L_i^{\pm}(k)$ and $L_r^{\pm}(k)$ for $k_F a = 4.3\pi$, $k_h a = 0.26\pi$ and $\xi_0/a = \infty$.

B. Majorana wavefunction

Consider a finite chain of N sites. Since the Majorana state $|\psi^M\rangle \in \ker g^{-1}(E=0)$, its real space representation in terms of a column vector $\psi^M(i) = \langle i|\psi^M\rangle$, with $i = 1, \dots N$, is in the kernel of the $8N \times 8N$ matrix g_{ij}^{-1} evaluated at $E = 0$. The occupation probability at site i is given by

$$\left|\psi^M(i)\right|^2 = \langle \psi^M(i), \psi^M(i)\rangle, \tag{41}$$

where $\langle \cdot, \cdot \rangle$ denotes the inner product in spin and particle-hole space. We then take either the components of the superconducting host when $\Gamma > \Delta$ or take the d components when $\Gamma < \Delta$. Note that the s and d entries have different units and cannot be added. However, the localization length of the end state is the same for both components.

C. Local density of states

The local density of states is related to the diagonal elements of

$$A^{\mu\nu}(\mathbf{r}, E) = -\frac{1}{\pi} \lim_{\eta \to 0^+} \mathrm{Im}\, \mathrm{Tr}_\sigma\, G^{\mu\sigma,\nu\sigma}(E + i\eta, \mathbf{r}, \mathbf{r}), \tag{42}$$

where $\mu, \nu \in \{s, d\} \times \{e, h\}$ are composite indices for (s,d) and (e,h) (particle-hole) components, and σ is the index of the spin space, within which the trace is taken. To obtain a true tunneling density of states, we would also need to use a Green function G which includes information about the spatial structure of the adatom d-states. This structure is not explicit in the Green function defined in Eq. (21). The latter treats the adatoms in tight-binding approximation and retains only the amplitudes of the atomic d-orbitals rather than the spatial structure of the corresponding wavefunctions.

In the case of $\Gamma \gg \Delta$, there is a strong transfer of the spectral weight of the subgap excitations to the superconductor. Therefore, apart from a narrow vicinity of the adatoms, the main contribution to the local density of states comes from the states of the host. In this limit, we neglect the contribution of the adatoms (i.e. the d-levels) to the local density of states. Focusing on the electron contribution, we compute $A^{\mu\nu}(\mathbf{r}, E)$ for $\mu = \nu = (s, e)$ and $\mathbf{r} = \mathbf{R}_j$ at site j. Explicitly, we are able to find the local density of states at each site j,

$$A_j(E) = A^{\mu\mu}(\mathbf{R}_j, E) = -\frac{1}{\pi} \lim_{\eta \to 0^+} \mathrm{Im}\, \mathrm{Tr}_\sigma\, g_{jj}^{\mu\sigma,\mu\sigma}(E + i\eta), \qquad \mu = (s, e), \tag{43}$$

from the lattice Green function g defined in Eq. (26). It should also be mentioned that we include a finite imaginary part in the energy $E \to E + i\eta$, with $\eta = 0.015\Delta$. This small η put in by hand introduces a finite broadening of the δ-peaks which we obtain from a finite size calculation. This results in a smooth local density of states.

V. DERIVATION OF EQUATION (9) IN THE MAIN TEXT

The dressed Green function of the superconductor including the self-energy from hybridization with the magnetic adatoms can be written as

$$g^{ss} = g_0^{ss}(1 - \Sigma g_0^{ss}). \tag{44}$$

The self-energy takes the form

$$\begin{aligned}\Sigma = t^2 g_0^{dd} &= \begin{pmatrix} E-\varepsilon_d^+ & KS & 0 & 0 \\ KS & E-\varepsilon_d^- & 0 & 0 \\ 0 & 0 & E+\varepsilon_d^+ & KS \\ 0 & 0 & KS & E+\varepsilon_d^- \end{pmatrix}^{-1} \\ &= \frac{t^2}{(E-\varepsilon_d^+)(E-\varepsilon_d^-)-(KS)^2}\begin{pmatrix} E-\varepsilon_d^- & -KS & 0 & 0 \\ -KS & E-\varepsilon_d^+ & 0 & 0 \\ 0 & 0 & 0 & 0 \\ 0 & 0 & 0 & 0 \end{pmatrix} + \frac{t^2}{(E+\varepsilon_d^+)(E+\varepsilon_d^-)-(KS)^2}\begin{pmatrix} 0 & 0 & 0 & 0 \\ 0 & 0 & 0 & 0 \\ 0 & 0 & E+\varepsilon_d^- & -KS \\ 0 & 0 & -KS & E+\varepsilon_d^+ \end{pmatrix}\end{aligned} \tag{45}$$

where $\varepsilon_d^{\pm}(k) = \epsilon_d - 2w\cos(k \pm k_h)$. We introduce $E_d^{\pm} = \varepsilon_d^{\pm} + KS$, and replace $\varepsilon_d^{\pm} = E_d^{\pm} - KS$ in the self-energy. Since $KS \gg E, E_d$, we can approximate

$$(E-\varepsilon_d^+)(E-\varepsilon_d^-) - (KS)^2 \simeq -KS(E_d^+ + E_d^- - 2E) \tag{46a}$$

$$(E+\varepsilon_d^+)(E+\varepsilon_d^-) - (KS)^2 \simeq -KS(E_d^+ + E_d^- + 2E) \tag{46b}$$

and

$$E \pm \varepsilon_d^{+,-} \simeq \mp KS. \tag{47}$$

Thus, for $KS \to \infty$, we find

$$\Sigma \simeq \frac{\alpha_-}{2\pi\nu_0}(1+\tau_z)(\sigma_x - \tau_z) + \frac{\alpha_+}{2\pi\nu_0}(1-\tau_z)(\sigma_x - \tau_z), \tag{48}$$

where

$$\alpha_\pm = \frac{\pi\nu_0 t^2}{2E_d \pm 2E}, \qquad E_d = \frac{E_d^+ + E_d^-}{2}. \tag{49}$$

Note that we can also write

$$\Sigma = e^{-i\frac{\pi}{4}\sigma_y}\left\{\frac{\alpha_-}{2\pi\nu_0}(1+\tau_z)(\sigma_z - \tau_z) + \frac{\alpha_+}{2\pi\nu_0}(1-\tau_z)(\sigma_z - \tau_z)\right\}e^{-i\frac{\pi}{4}\sigma_y} = e^{i\frac{\pi}{4}\sigma_y}\begin{pmatrix} 0 & 0 & 0 & 0 \\ 0 & -\frac{2\alpha_-}{\pi\nu_0} & 0 & 0 \\ 0 & 0 & \frac{2\alpha_+}{\pi\nu_0} & 0 \\ 0 & 0 & 0 & 0 \end{pmatrix} e^{-i\frac{\pi}{4}\sigma_y}. \tag{50}$$

Then

$$\begin{aligned}\det(1-\Sigma g_0^{ss}) &= \det\left\{1 - \begin{pmatrix} 0 & 0 & 0 & 0 \\ 0 & -\frac{2\alpha_-}{\pi\nu_0} & 0 & 0 \\ 0 & 0 & \frac{2\alpha_+}{\pi\nu_0} & 0 \\ 0 & 0 & 0 & 0 \end{pmatrix}\begin{pmatrix} \mathcal{A}+\mathcal{B} & \mathcal{E}+\mathcal{F} & \mathcal{C} & \mathcal{D} \\ \mathcal{E}+\mathcal{F} & \mathcal{A}+\mathcal{B} & \mathcal{D} & \mathcal{C} \\ \mathcal{C} & \mathcal{D} & \mathcal{A}-\mathcal{B} & -\mathcal{E}+\mathcal{F} \\ \mathcal{D} & \mathcal{C} & -\mathcal{E}+\mathcal{F} & \mathcal{A}-\mathcal{B} \end{pmatrix}\right\} \\ &= \det\left\{1 - 2\begin{pmatrix} -\alpha_-(\mathcal{A}+\mathcal{B}) & -\alpha_-\mathcal{D} \\ \alpha_+\mathcal{D} & \alpha_+(\mathcal{A}-\mathcal{B}) \end{pmatrix}\right\} \\ &= [1+2\alpha_-(\mathcal{A}+\mathcal{B})]\,[1-2\alpha_+(\mathcal{A}-\mathcal{B})] + 4\alpha_+\alpha_-\mathcal{D}^2 \\ &= 1 + 2\mathcal{A}(\alpha_- - \alpha_+) + 2\mathcal{B}(\alpha_- + \alpha_+) + 4\alpha_+\alpha_-(\mathcal{D}^2 + \mathcal{B}^2 - \mathcal{A}^2)\end{aligned} \tag{51}$$

where

$$\mathcal{A} = \frac{E}{\sqrt{\Delta^2 - E^2}} L_i \qquad \mathcal{B} = L_r \qquad \mathcal{C} = \frac{\Delta}{\sqrt{\Delta^2 - E^2}} L_i \tag{52}$$

$$\mathcal{D} = -\frac{\Delta}{\sqrt{\Delta^2 - E^2}} (\delta L_i) \qquad \mathcal{E} = -(\delta L_r) \qquad \mathcal{F} = -\frac{E}{\sqrt{\Delta^2 - E^2}} (\delta L_i) \tag{53}$$

and

$$L_{i,r} = \frac{L^+_{i,r} + L^-_{i,r}}{2} \qquad (\delta L_{i,r}) = \frac{L^+_{i,r} - L^-_{i,r}}{2}. \tag{54}$$

The excitation spectrum can be obtained by requiring the above determinant to be zero,

$$\begin{aligned} 0 &= 1 + \frac{2E}{\sqrt{\Delta^2 - E^2}} L_i(\alpha_- - \alpha_+) + 2L_r(\alpha_- + \alpha_+) + 4\alpha_+\alpha_- \left\{ \frac{\Delta^2}{\Delta^2 - E^2} (\delta L_i)^2 - \frac{E^2}{\Delta^2 - E^2} L_i^2 + L_r^2 \right\} \\ &= 1 + \frac{2\Gamma E_d}{E_d^2 - E^2} L_r + \frac{\Gamma^2}{E_d^2 - E^2} L_r^2 \\ &+ \frac{2E^2}{\sqrt{\Delta^2 - E^2}} \frac{\Gamma}{E_d^2 - E^2} L_i + \frac{\Gamma^2}{E_d^2 - E^2} \left\{ \frac{\Delta^2}{\Delta^2 - E^2} (\delta L_i)^2 - \frac{E^2}{\Delta^2 - E^2} L_i^2 \right\} \end{aligned} \tag{55}$$

with $\Gamma = \pi \nu_0 t^2$. Multiplying by $(\Delta^2 - E^2)(E_d^2 - E^2)$ gives Eq. (9) of the main text,

$$(\Delta^2 - E^2)[E_d + \Gamma L_r]^2 - E^2[\sqrt{\Delta^2 - E^2} - \Gamma L_i]^2 + \Gamma^2 \Delta^2 (\delta L_i)^2 = 0. \tag{56}$$